Catalytic co-hydrothermal carbonization of food waste digestate and yard waste for energy application and nutrient recovery

Catalytic co-hydrothermal carbonization of food waste digestate and yard waste for energy application and nutrient recovery

Mingjing He [a,b], Xiefei Zhu [a,b], Shanta Dutta [a,b], Samir Kumar Khanal [c], Keat Teong Lee [d], Ondrej Masek [e], Daniel C.W. Tsang [a,b*]

[a] Department of Civil and Environmental Engineering, The Hong Kong Polytechnic University, Hung Hom, Kowloon, Hong Kong, China

[b] Research Centre for Resources Engineering towards Carbon Neutrality, The Hong Kong Polytechnic University, Hung Hom, Kowloon, Hong Kong, China

[c] Department of Molecular Biosciences and Bioengineering, University of Hawai‘i at Mānoa, Honolulu, HI, USA

[d] School of Chemical Engineering, Universiti Sains Malaysia, Engineering Campus, Seri Ampangan, Nibong Tebal 14300, Pulau Pinang, Malaysia

[e] UK Biochar Research Centre, School of Geosciences, University of Edinburgh, Alexander Crum Brown Road, Crew Building, EH9 3FF, Edinburgh, UK

* Corresponding author: **dan.tsang@polyu.edu.hk**

Graphical Abstract

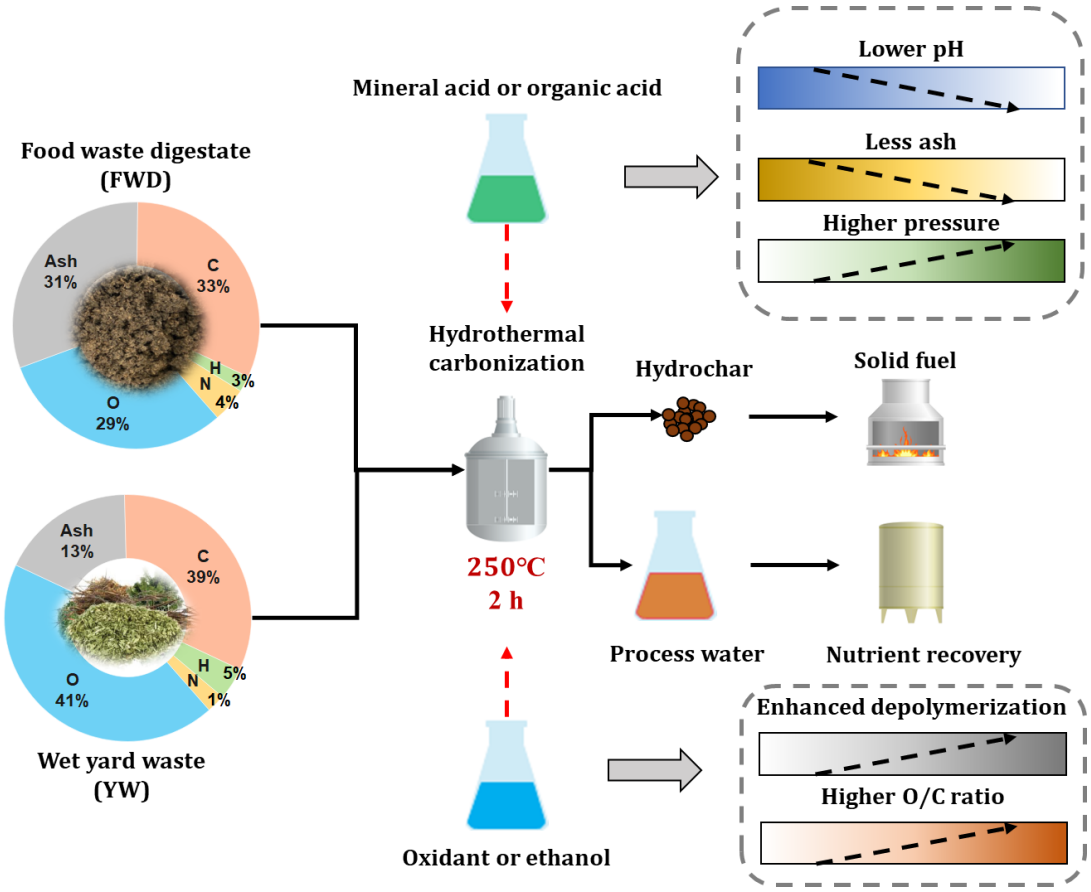

Abstract

Hydrothermal carbonization (HTC) provides a promising alternative to valorize food waste digestate (FWD) and avoid disposal issues. Although hydrochar derived from FWD alone had a low calorific content (HHV of 13.9 MJ kg^{-1}), catalytic co-HTC of FWD with wet lignocellulosic biomass (*e.g.*, wet yard waste; YW) and 0.5 M HCl exhibited overall superior attributes in terms of energy recovery (22.7 MJ kg^{-1}), stable and comprehensive combustion behaviour, potential nutrient recovery from process water (2-fold higher N retention and 129-fold higher P extraction), and a high C utilization efficiency (only 2.4% C loss). In contrast, co-HTC with citric acid provided ~3-fold higher autogenous pressure, resulting in a superior energy content of 25.0 MJ kg^{-1}, but the high C loss (~74%) compromised the overall environmental benefits. The results of this study established a foundation to fully utilize FWD and YW hydrochar for bioenergy application and resource recovery from the process water.

Keywords: Food waste hydrochar; Yard waste recycling; Resource recovery; Bioenergy; Solid fuel; Sustainable waste management.

1 Introduction

Globally, ~17% of produced food is lost or wasted, which is equivalent to 8−10% of total greenhouse gases (GHGs) emissions (UNEP, 2021). To tackle the increasing global food waste generation and associated management/disposal issues, anaerobic digestion (AD) is a widely adopted technology to recover biogas from food waste, while the resulting residues (referred as food waste digestate (FWD)) remains largely underutilized due to low economic and environmental benefits (Dutta et al., 2021; Parmar and Ross, 2019). The FWD is a metal-free and semi-stabilized mixture consisting of high moisture content, less degradable organic matter (mainly cellulose and lignocellulose), nutrients, minerals, and microbial cells, etc. (Dutta et al., 2021). Currently available options such as composting or direct application to soil as a biofertilizer are often limited by the local market volume and strict requirements, and they would also contribute to high GHGs emissions, odour nuisance, nutrient leaching, pathogen exposure, and potential phytotoxic responses (Ahmed et al., 2021; Coelho et al., 2018). Herein, beyond direct soil application of FWD or its compost, hydrothermal carbonization (HTC) as a thermochemical treatment in subcritical aqueous media (180−250 °C) with auto-generated pressure has emerged as a potentially promising approach to convert wet biomass to hydrochar. Compared with conventional pyrolysis for FWD, HTC process would eliminate the need of energy-intensive drying process as a prerequisite and produce carbon-enriched hydrochar with favourable energy density for bioenergy (in the form of solid fuel) and various environmental applications (Cao et al., 2021; Yang et al., 2020).

Different from the HTC of lignocellulosic biomass into hydrochar, the HTC of AD digestate failed to densify the bioenergy for the solid fuel application of hydrochar in previous studies, and low HHVs ranging from 8 to 13 MJ kg^{-1} were reported due to insufficient carbonization process and low content of recalcitrant carbon in the digestate feedstock (Dutta et al., 2021; Merzari et al., 2020; Zhang et al., 2021). It is noted that recent HTC studies have demonstrated promising results for various feedstock, *e.g.,* food waste (Sharma and Dubey, 2020), sewage sludge (Wilk et al., 2021), and animal manure (Lang et al., 2019)). In this context, co-HTC of FWD with lignocellulosic biomass such as wet yard waste (YW) may improve the energy recovery from FWD and simultaneously avoid the disposal issues of wet YW. Moreover, the lignin in YW may facilitate the solid particle bridging and interlocking of bulky particles within the hydrochar, thus possibly improving the mechanical durability and handling process of hydrochar pellet product (Sharma and Dubey, 2020). Owing to the specific properties of FWD, the efficacy of co-HTC of FWD and YW on energy recovery and combustion behaviour is still unknown.

HTC undergoes a series of reactions to produce hydrochar as the solid product, including depolymerization to intermediates *via* hydrolysis, dehydration, decomposition, decarboxylation, and deamination, followed by repolymerization and condensation (Liu et al., 2021; Nicolae et al., 2020). Different catalysts could be applied to enhance the properties of hydrochar by facilitating specific HTC reaction pathways with less energy consumption. Acidic conditions of HTC process could facilitate the biomass depolymerization processes (hydrolysis, dehydration, and deamination) by the release of hydrogen ions (Yang et al., 2020). Oxidants

74 such as H_2O_2 and HNO_3 could destruct biomass to smaller molecules by bond cleavage and
75 oxidation, which might promote the subsequent repolymerization (Qian et al., 2015). Organic
76 acids (*e.g.,* acetic acid) could not only create an acidic environment but also provide additional
77 substrates for repolymerization and hydrochar formation. Moreover, as organic acids were the
78 main intermediates decomposed from polysaccharides and monomers (Mäkelä and Yoshikawa,
79 2016; Nicolae et al., 2020), applying organic acid as a catalyst could provide additional
80 scientific insights on the potential of recycling the process water to HTC process. In addition,
81 the application of water-solvent system could increase the severity of HTC reaction due to the
82 lower critical temperature, which would augment the depolymerization process by dissolving
83 large molecules to liquid (Yang et al., 2021). The active hydrogen donated by polar solvents
84 (*e.g.*, ethanol and methanol) could facilitate the dehydration reaction (Liu et al., 2021), which
85 is suitable for biomass feedstock with high protein and carbohydrate contents such as FWD.
86 Hence, we attempted to simultaneously address the FWD and YW disposal issues by valorizing
87 them as a source for renewable energy (hydrochar) and resource recovery (process water).
88 In this study, FWD and YW were mixed for co-HTC process with organic catalytic systems
89 (using organic acids and/or solvents) and inorganic catalytic systems (using mineral acids
90 and/or oxidants). The produced hydrochar was characterized for the possible catalytic effects;
91 various fuel properties (*e.g.,* compositions, energy properties, and combustion behaviour) of
92 hydrochar were determined. The characteristics of process water were evaluated for potential
93 nutrient recovery and wastewater recycling. The carbon balance and operation pressure, which

have been overlooked in most of the previous studies, were also investigated to reveal the carbon utilization efficiency and the effect of autogenous pressure on hydrochar production.

2 Materials and methods

2.1 Materials

The biomass feedstock of interest is the locally generated food waste digestate (FWD) and wet yard waste (YW, a mixture of fallen leaves, grass clippings, and small branches) collected from the O•PARK1 and the EcoPark in Hong Kong, respectively. The collected biomass waste was oven-dried at 105 ℃ until constant weight to determine the moisture content; and the samples were crushed to pass an 18-mesh (1 mm) and sealed in an air-tight container before further analysis. In practical applications, this drying process is not required. The properties of YW and FWD were determined according to **Section 2.3**. All the chemicals used in this study were of analytical grade.

2.2 Hydrothermal carbonization

For each HTC process, 35 g of feedstock was mixed with 350 mL of solution (10% solid loading rate) to maintain the solubilized chemical species and homogeneity of HTC reactions. FWD and YW were mixed with a mass ratio of 1:1 for the co-HTC process, namely “Mix”. Different catalytic systems were prepared for the co-HTC process, namely, system without catalyst (deionized (DI) water), organic catalytic system (1 M acetic acid, 1 M citric acid, 1 M

112 citric acid with 1% H_2O_2, and 10 wt.% ethanol-water system), and mineral acid catalytic system
113 (*i.e.,* 0.1 M HCl, 0.1 M HCl with 1% H_2O_2, 0.5 M HCl, 0.1 M HNO_3, and 0.5 M HNO_3).

114 The HTC process was performed in a 500-mL Parr bench top reactor (Parr 4575A, USA)
115 with eight compression bolts for flat gaskets. The reactor was heated to 250±5 ℃ at
116 approximately 9 ℃ min^{-1} (power of 1800 W; ramping time of 26−28 min to reach the target
117 temperature) and held for 2 h with a stirring speed of 300±2 rpm. The temperature of 250 ℃
118 was selected as it is critical to protein hydrolysis with a higher water dissociation constant
119 (Yang et al., 2020). The holding time of 2 h was chosen as a shorter residence time may lead
120 to insufficient repolymerization process and lower refractory carbon content, while prolonging
121 the residence time would have an adverse impact on the solid yield and energy content (Lucian
122 et al., 2018). During the heating and holding stages, the temperature and auto-generated
123 pressure were continuously monitored. After the heating process, the reactor was cooled to
124 room temperature (~1 h) by tap water through an installed single-loop cooling coil and the
125 auto-generated pressure was released by the pressure release valve. The HTC slurry was filtered
126 through a vacuum filter (0.45-μm), the separated hydrochar was oven-dried at 60 ℃ for 24 h
127 and weighted for yield calculation (**Eq. 1**), then sealed for further analysis. The separated
128 process water was collected and stored at 4 ℃ in the dark without dilution for further analysis.

129 $$\text{Yield } (/) = \frac{m_{hydrochar}}{m_{feedstock}} \quad \textbf{Eq. 1}$$

130 where $m_{hydrochar}$ (g) is the dry mass of hydrochar and $m_{feedstock}$ (g) is the dry mass of feedstocks.

2.3 Characterization of feedstock and hydrochar

2.3.1 Composition analysis

The elemental composition (C, H, N and S; wt.% dry basis) of samples was determined by an elemental analyzer (EA, Vario EL cube, Germany) with random duplication. The proximate analysis (ash content, volatile matter (VM), and fixed carbon (FC; calculated by difference); wt.% dry basis) was carried out according to ASTM D1762-84 standard in duplicates or triplicates. The O content was calculated by **Eq. 2**. The fuel ratio (FR) and fixed carbon recovery (FCR) of hydrochar were calculated by **Eq. 3** and **Eq. 4**, respectively.

$$[\mathrm{O}]\ (\mathrm{wt.\,\%\ dry\ basis}) = 100 - [\mathrm{C}] - [\mathrm{H}] - [\mathrm{N}] - [\mathrm{S}] - \mathrm{ash} \qquad \textbf{Eq. 2}$$

$$\mathrm{FR}\ (/) = \frac{\mathrm{FC}}{\mathrm{VM}} \qquad \textbf{Eq. 3}$$

$$\mathrm{FCR}\ (/) = \frac{\mathrm{FC_{hydrochar}}}{\mathrm{FC_{feedstock}}} \times \mathrm{Yield} \qquad \textbf{Eq. 4}$$

To predict the likelihood of fouling during combustion, the total metal contents of hydrochar were determined by a modified USEPA Method 3050B where the hydrochar was digested by concentrated HNO_3/H_2O_2. The digested samples were diluted by 5% HNO_3 and filtered (0.45-μm) prior to the analysis, then measured by an inductively coupled plasma optical emission spectroscopy (ICP-OES, Spectro). The combustion alkali index was calculated using **Eq. 5** (Smith et al., 2016).

$$\mathrm{CAI} = \frac{\mathrm{K_2O + Na_2O}}{\mathrm{HHV_{hydrochar}}} \times 10^3 \qquad \textbf{Eq. 5}$$

where K_2O (kg kg^{-1} hydrochar) and Na_2O (kg kg^{-1} hydrochar) were calculated based on the total digestion results from ICP-OEC; $HHV_{hydrochar}$ (MJ kg^{-1}) is the higher heating value of hydrochar determining according to **Section 2.3.2.**

2.3.2 Thermal analysis

The combustion experiments of hydrochar were conducted with a Thermogravimetric Analyzer-Differential Scanning Calorimeter (TG-DSC; PerkinElmer Pyris1) in an air flow environment. The differential thermogravimetric (DTG) data was analyzed based on the TG-DSC results. Approximately 5 mg of sample was loaded into an Al_2O_3 crucible, the thermal analysis started from 30 ℃ with a ramping rate of 20 ℃ min^{-1} to 900 ℃. The TG-DSC and DTG results provided the characteristic combustion parameters to reveal the combustion behaviour of the hydrochar samples, including comprehensive combustion index (CCI) and combustion stability index (R_w) calculated by **Eq. 6** and **Eq. 7**, respectively (Lang et al., 2019; Sharma and Dubey, 2020). The ignition temperature (T_i) was defined as the temperature of the combustion rate increased to 1 wt.% min^{-1}. The burnout temperature (T_b) was defined as the temperature at which combustion rate decreased to 1 wt.% min^{-1} (Ro et al., 2019). To investigate the interactions between FWD and YW during the catalytic co-HTC process, the theoretical TD curve of Mix_DI was calculated by **Eq. 8** (Xie et al., 2018). The HHVs of feedstock and hydrochar were determined using an oxygen bomb calorimeter (KA921D; HEBI Coal I&M Co. Ltd.) according to the ASTM D5865-13 standard. The energy densification E_d

(**Eq. 9**) (Lang et al., 2019) and energy recovery E_r (**Eq. 10**) were calculated to reveal the energy-related properties of hydrochar.

$$CCI = \frac{DTG_m \times DTG_{mean}}{T_i^2 \times T_b} \quad \textbf{Eq. 6}$$

$$R_w = 8.5875 \times 10^7 \times \frac{DTG_m}{T_i \times T_m} \quad \textbf{Eq. 7}$$

$$TG_{theo} = x_{FWD} \times TG_{FWD\_DI} + x_{YW} \times TG_{YW\_DI} \quad \textbf{Eq. 8}$$

$$E_d = \frac{HHV_{hydrochar}}{HHV_{feedstock}} \quad \textbf{Eq. 9}$$

$$E_r = \frac{m_{solution} \times C_{p\ solution} \times \Delta T + m_{feedstock} \times (C_{p\ feedstock} \times \Delta T + HHV_{feedstock})}{m_{feedstock} \times yield \times HHV_{hydrochar}} \quad \textbf{Eq. 10}$$

where DTG_m and DTG_{mean} are the maximum and average weight loss rates; T_i, T_b, and T_m represent ignition temperature, burnout temperature, and peak temperature of DTG_m, respectively; x_{FWD} and x_{YW} refer to the mass fractions of FWD and YW; TG_{FWD_DI} and TG_{YW_DI} are the TG curves of hydrochar FWD_DI and YW_DI; $m_{solution}$ and $m_{feedstock}$ are the mass of solution and feedstocks, respectively; $C_{p\ solution}$ and $C_{p\ feedstock}$ are the specific heat capacity (4.18 $kJ^{-1}\ kg^{-1}\ °C^{-1}$ for water; 2.46 $kJ^{-1}\ kg^{-1}\ °C^{-1}$ for ethanol; assumed 2.5 $kJ^{-1}\ kg^{-1}\ °C^{-1}$ for feedstocks (Faitli et al., 2015)); ΔT is the temperature difference (250 – 25 = 225 °C).

2.4 Analysis of process water

The total organic carbon (TOC) and total nitrogen (TN) in the process water was analyzed by a TOC-L/TN analyzer (Shimadzu Corporation). The total phosphate (PO_4^{3-}) content was measured by PhosVer 3 Method with phosphate reagent power pillows, then the concentrations were determined by a colorimeter (HACH). The $SUVA_{254}$ and E_2/E_3 ratio of process water were

calculated by **Eq. 11** and **Eq. 12** to unveil the aromaticity and molecular weight of process water (e.g., higher E_2/E_3 ratio indicates lower molecular weight) based on the UV-vis absorbance value measured using a UV-vis spectrophotometer (200-700 nm with 0.5-nm interval) (McCabe and Arnold, 2018).

$$SUVA_{254} = \frac{2.303A_{254}}{I_L \times TOC} \quad \textbf{Eq. 11}$$

$$\frac{E_2}{E_3} = \frac{A_{250}}{A_{365}} \quad \textbf{Eq. 12}$$

where A_{254} is the absorbance at 254 nm, I_L is the path-length of the optical cell in meters (l = 0.01 m). TOC is the total organic carbon content in process water. A_{250} and A_{365} are the absorbance at 250 nm and 365 nm, respectively.

3 Results and discussion

3.1 Hydrochar characteristics

As shown in **Table 1**, **Figure 1a-b** and the Van Krevelen diagram (**Figure 2**), the elemental contents of hydrochar were remarkably affected by the feedstock types and catalytic systems. Similar to recent studies on digestate-derived hydrochar (Aragón-Briceño et al., 2020; Parmar and Ross, 2019), owing to the limited lignin content and high ash content in FWD (30.5%), HTC of FWD alone without catalyst (FWD_DI) resulted in an ineffective carbonization process only with a slight increase in C content (from 32.9% to 34.4%) and atomic H/C ratio (from 1.09 to 1.24), and a decrease in FC content (from 3.4% to 1.2%). The decrease in O content (from 29.4% to 12.0%) suggested that dehydration and decarboxylation would be the

207 major reactions for FWD_DI (Nicolae et al., 2020). By contrast, HTC of YW under the same
208 conditions revealed a notable rise in C content from 39.4% in YW to 54.5% in YW_DI, which
209 could be attributed to the higher lignin content of YW that creates an energy barrier hindering
210 the release of volatiles during HTC process (Zhang et al., 2018). After co-HTC of mixed FWD
211 and YW, most compositional values of Mix_DI were close to the average values of that of
212 FWD_DI and YW_DI, except for the fixed carbon of 11.6% (8.2% for the calculated average
213 value). This suggested that the lignin in YW could provide possible condensation sites for
214 enhancing interparticle bonding and bridging (Sharma et al., 2020).

215 By using organic acids (acetic acid or citric acid) as catalysts in the co-HTC process, the
216 C content was effectively augmented from 44.1% (Mix_DI) to 51.6% (Mix_Acetic) and 57.6%
217 (Mix_Citric), which was ascribed to the accelerated hydrolysis process and the decomposition
218 of biopolymers, hence enhancing the hydrochar formation. By contrast, the hydrochar
219 produced from co-HTC with water-ethanol system (Mix_Ethanol) revealed a lower C content
220 (43.7%). The hydrochar formation was possibly limited by the inhibited repolymerization
221 process and enhanced dissolution of organic compounds by solvolysis in ethanol (Yang et al.,
222 2021). A high atomic O/C ratio of 0.41 was manifested for Mix_Ethanol, indicating that the
223 hydrochar possessed a lower carbon stability but more abundant surface functional groups for
224 environmental applications such as metal immobilization (Xu et al., 2021a). Regarding the
225 catalytic systems with mineral acids, a low concentration (0.1 M HCl or HNO_3) revealed an
226 insufficient catalytic effect on the carbonization process with only 2−4% of enrichment of C
227 content. The co-HTC process with 0.5 M HCl exhibited an effective acid catalysis resulting in

a high C content of 57.5% (1.3-fold of Mix_DI). Nevertheless, for the co-HTC process with 0.5 M HNO_3, oxidation was found to be dominant that the C content significantly decreased to 38.6% with the highest atomic O/C ratio of 0.47.

The combustion alkali index (CAI) is an important indicator of solid fuel slagging potential (Smith et al., 2016), the CAI values of all the hydrochar samples in this study were within the safe combustion threshold of 0.17 (**Figure 1c**). Apart from the hydrochar catalyzed by HNO_3, the CAI of hydrochar was positively correlated to the ash content (R^2 = 0.84), which was mainly controlled by the initial pH of process water. It was found that although HNO_3 could increase the acidity of HTC process, the ash contents for Mix_0.1 M HNO_3 and Mix_0.5 M HNO_3 remained ~31%, possibly because the newly dissolved mineral cations (from ash components) were subjected to surface complexation with the enriched oxygen-containing functional groups on the hydrochar surface (Zheng et al., 2021). The stability of hydrochar as a solid fuel could be revealed by FR and FCR (**Figure 1d**), a value of FR lower than 0.33 denoted a non-stable hydrochar with a half-life less than 100 years (Sztancs et al., 2021). Hydrochar catalyzed by 0.5 M HCl or HNO_3 exhibited medium stability with FR higher than 0.33. The highest values of FR (0.62; 3.0-fold of Mix_DI) and FCR (1.47; 2.5-fold of Mix_DI) were reported for Mix_0.5 M HNO_3, probably owing to the oxidation of labile carbon during HTC process, as manifested by the highest FC content (26.4%).

3.2 Thermal analysis of hydrochar

As illustrated in **Figure 3**, HTC process was more effective to densify energy for YW_DI (HHV = 20.7 MJ kg^{-1}) with E_d of 1.24 than that of FWD_DI with only 1.05 of E_d (HHV = 13.9 MJ kg^{-1}) owing to the high ash content and low recalcitrant carbon content in FWD. The co-HTC of FWD and YW showed an improvement on the energy densification for Mix_DI with E_d of 1.26. Nevertheless, in view of the HHV for commercial solid fuel (*e.g.,* 26.2 MJ kg^{-1} for coking coal (Dincer et al., 2018)), the application of Mix_DI as a solid fuel might still be hindered by the relatively low HHV (18.9 MJ kg^{-1}) and high ash content (33.4%). In this context, catalytic systems were deployed to improve the HHV and energy-related performance of hydrochar.

The co-HTC using acetic acid, citric acid, and HCl could increase the HHV compared to the non-catalytic HTC (1.04- to 1.33-fold of Mix_DI). Mix_Citric obtained the largest increase in HHV (25.0 MJ kg^{-1}), E_d (1.67), and E_r (0.50), probably because citric acid as a tricarboxylic acid had a high capacity to accelerate the hydrolysis of biomass into smaller fragments, and the enhanced repolymerization process increased the yield of hydrochar (Faradilla et al., 2020). However, the addition of H_2O_2 and HNO_3 had adverse effects on the HHV value (0.6-3.7 MJ kg^{-1} reduction) due to the oxidation of biomass, reflected by the higher atomic O/C ratio in **Figure 1** and **2**. Although the hydrochar catalyzed by the water-ethanol system (Mix_Ethanol) displayed the highest solid yield (0.56), it had a lower HHV (17.3 MJ kg^{-1}) probably owing to the dissolution of high-molecular-weight organic compounds by ethanol (Zhang and Zhang, 2014). It is noteworthy that for the hydrochar with similar ash content (**Figure 1c**), a lower

HHV would result in a higher CAI. For instance, Mix_0.5 M HNO_3 with HHV of 15.1 MJ kg^{-1} exhibited a higher CAI (0.16) than that of Mix_0.1 M HNO_3 (HHV = 18.5 MJ kg^{-1}; CAI = 0.11).

3.3 Combustion behaviour and characteristics of hydrochar

The combustion behaviour of hydrochar can be revealed by TG-DSC and DTG analysis (**Figure 4**). The combustion parameters (DTG_m, DTG_{mean}, T_m, T_i, and T_b) and the calculated values of CCI and R_w for energy application potential of hydrochar are summarized in **Table 2.** As depicted in **Figure 4**, three stages of combustion weight loss were identified, including (1) loss of inherent bound water and release of light volatiles (< 170 ℃), (2) main stage of combustion with thermal decomposition of macromolecular organic matter and further release of volatiles (170-550 ℃), and (3) slow combustion stage for ash fusion (550-750 ℃).

In the absence of catalysts, the combustion behaviour and energy performance of hydrochar were mainly controlled by the feedstock compositions. As shown in **Figure 4a-b**, the high DTG_m of 11.4 wt.% min^{-1} at 411 ℃ and the double DSC peaks of YW_DI suggested the enrichment of lignin with intensive combustion activity (Xu et al., 2021b). Compared with YW_DI, the earlier peak of FWD-derived hydrochar (FWD_DI; T_m = 319 ℃) revealed that hemicellulose and cellulose and their derived oligomers could be the main constituents in FWD_DI, as the DTG peaks centred at approximately 290 ℃ and 350 ℃ could be predominately attributed to the hemicellulose and cellulose decomposition, respectively (Lane et al., 2018). A synergistic effect was observed for co-HTC hydrochar (Mix_DI) by comparing

287 the actual and the theoretical TG and DTG curves (**Figure 4a**), the reaction homogeneity for
288 biomass with different constituents was enhanced by the co-HTC process that the theoretical
289 two peaks were merged into one peak (**Figure 4b**). Moreover, compared with YW_DI, the
290 presence of FWD in co-HTC process delayed the T_i to 240 ℃ due to the lower content of VM
291 (55.0% for Mix_DI vs 64.8% for YW_DI), which corresponded to a lower risk of fire and
292 explosion of the hydrochar during transportation and handling process (Lang et al., 2019).
293 In organic catalytic co-HTC processes (**Figure 4c&d** and **Table 2)**, the addition of acetic
294 acid or citric acid was found effective to enhance the thermal stability of hydrochar with a delay
295 of the T_m to 384 ℃ and 407 ℃ and an increase of the CCI to 1.6- and 4.0-fold of that of Mix_DI,
296 respectively. Nevertheless, hydrochar catalyzed by water-ethanol system (Mix_Ethanol)
297 experienced a contrary trend with an additional earlier DTG peak at 301 ℃ and a lower CCI
298 of 2.9. This was probably attributed to the ring-opening and hydrogenation reactions and the
299 inhibited repolymerization process of the dispersed organic fragments in ethanol solvent (Yang
300 et al., 2021). In other words, the derived hydrochar was less stable with an earlier DSC peak
301 (**Figure 4d**). Regarding the hydrochar manufactured in the presence of H_2O_2 or HNO_3
302 oxidation, an earlier DTG peak at 283−294 ℃ suggested the decomposition of biomass. As
303 illustrated in **Figure 4e-h**, hydrochar catalyzed by 0.5 M HCl (Mix_0.5 M HCl) manifested the
304 highest DTG_m (15.6 wt.% min^{-1}) at 384 ℃ with superior values of CCI (14.2) and R_w (18.1),
305 suggesting the outstanding combustion stability with comprehensive heat release properties. In
306 comparison, a low concentration of mineral acid (0.1 M HCl or 0.1 M HNO_3) endowed little

influence on the combustion behaviour of hydrochar but slightly augmented the CCI to 6.2 and 5.4, respectively.

Interestingly, a small DTG peak at 550−750 ℃ was observed for some hydrochar samples in **Figure 4**, probably caused by the ash fusion of hydrochar. A positive correlation (R^2 = 0.80) was found between the ash content and the maximum DTG of 550−750 ℃ ($DTG_{m550-750}$), which could be attributed to the salt melting (mainly Ca salts) in the hydrochar (Yuan et al., 2017). This observation was validated by the ICP-OES analysis of the total metal contents of hydrochar samples. It was found that the Ca content in hydrochar was positively correlated (R^2 = 0.85) to $DTG_{m550-750}$, while this trend was hardly observed for other metals (*i.e.,* Fe, K, Mg, and Na; $R^2 < 0.52$). Similar DTG peaks were reported for hydrochar derived from other types of Ca-rich feedstock (Mäkelä and Yoshikawa, 2016; Yuan et al., 2017).

In a nutshell, ash content and mineral constituents were the decisive factors for the energy application potential of hydrochar according to the Pearson Correlation, the intensity and position of peaks were affected by the hydrochar constituents with negative correlation for DTG_{mean} and ash content (R^2 = 0.72), T_i and VM content (R^2 = 0.65), respectively. The presence of Ca in hydrochar would lead to a higher burnout temperature (T_b) with a lower CCI.

3.4 Characterization of process water

The process water resulting from the HTC process often contains high concentrations of dissolved organic compounds (volatile fatty acids, furan derivatives, carboxylic acids, etc.) and nutrients (*e.g.,* N and P), which can be applied for resource recovery or directly recycled for a

new batch of HTC process or downstream anaerobic digestion process for additional bioenergy generation (Dutta et al., 2021; Nicolae et al., 2020). In this context, understanding the characteristics of process water can reveal the potential for full utilization. As depicted in **Figure 5a**, without the addition of catalysts, depending on the compositions of feedstock, the nutrients extraction into the process water were 0.5−2.6 g TN L^{-1} (63.5% for FWD_DI, 50.1% for YW_DI, and 50.0% for Mix_DI) and 0.01−0.04 g PO_4^{3-} L^{-1}, respectively. The process water of Mix_0.5 M HCl resulted in the highest extraction of TN (2.6 g L^{-1}; 1.5-fold of Mix_DI) and PO_4^{3-} (2.58 g L^{-1}; 129-fold of Mix_DI), which provided a promising potential for further resource recovery (*e.g.,* struvite precipitation for P recovery and further use of process water as a N source) (Deng et al., 2020; Zhang et al., 2020). This could be attributed to acid-promoted leaching of inorganic stable P and dissolution and decomposition of organic-N in the feedstock (Marin-Batista et al., 2020). The characteristics of dissolved organic carbon in the process water are illustrated in **Figure 5b**. In non-catalytic systems, YW_DI possessed a higher TOC content of 11.7 g L^{-1} and E_2/E_3 ratio of 13.7, suggesting that the organic compounds in the process water had a lower molecular weight on average. Organic catalytic co-HTC resulted in a much higher TOC of 33.8−50.3 g L^{-1} with lower aromaticity ($SUVA_{254}$ = 0.6−1.5 L mg^{-1} m^{-1}) of the process water, owing to the C addition from organic acids or ethanol. Without the additional C source, Mix_0.5 M HNO_3 also exhibited a high TOC of 26.3 g L^{-1} (2.8-fold of Mix_DI) with low aromaticity ($SUVA_{254}$ = 1.0 L mg^{-1} m^{-1}), possibly due to the decomposition and oxidation of biopolymers into lower-molecular-weight organic compounds (E_2/E_3 = 9.7) (McCabe and Arnold, 2018).

3.5 Carbon balance and operation pressure

As shown in **Figure 6a**, compared with YW_DI (3.6% C loss), a higher C loss in the gas phase (~18% C loss) was observed for FWD_DI and Mix_DI, probably due to the thermal decomposition of labile carbon in FWD to CO_2. Regarding the organic catalytic co-HTC process, although additional carbon source was deployed, a remarkable C loss was observed for Mix_Acetic and Mix_Ethanol (50−60%) and ~74% for citric acid catalyzed hydrochar, which could be attributed to the thermal decomposition of organic acids or ethanol (easily degradable organics) to CO_2 (Wyrzykowski et al., 2011). By contrast, co-HTC with 0.5 M HCl exhibited the highest C retention (70.3%) in the hydrochar with only 2.4% of C loss, revealing the superior C utilization efficiency during the hydrochar formation. The operation pressure during HTC process (holding stage) is illustrated in **Figure 6b-c**. The pressure was maintained approximately 4.1−4.3 MPa for most of the HTC processes, which was slightly higher than the saturated pressure of water at 250℃ (4.0 MPa) due to the solid loading and the decomposition of organic compounds in the feedstock (CRC, 2005). Interestingly, a significantly higher pressure of 11.7−12.2 MPa for citric catalyzed co-HTC was observed at the end of holding stage, probably resulting from the thermal decomposition of citric acid to CO_2 (decomposition temperature of 175−250 ℃ (Wyrzykowski et al., 2011)). This observation could correspond to the higher C loss (**Figure 6a)** and the higher HHV value compared with the hydrochar catalyzed by strong mineral acid (0.5 M HCl), which was in line with the higher extent of repolymerization process (**Figure 3**). Regarding the hydrochar catalyzed by 0.5 M HNO_3, the high operation pressure (8.2 MPa) could be owing to the thermal decomposition of HNO_3 to

369 NO_2 in the gas phase with 72% of N loss. The high N content (3.3%) in the hydrochar might
370 also arouse concerns of NO_x emissions during combustion.

371 **3.6 Hydrochar for energy and environmental applications**

372 Depending on the target applications of hydrochar, co-HTC with 0.5 M HCl could be the
373 recommended strategy for solid fuel production and nutrient recovery by achieving (1) stable
374 (FR > 0.33; stable half-life > 100 years) and comprehensive combustion properties (CCI = 14.2;
375 R_w = 18.1) for hydrochar with HHV of 22.7 MJ kg^{-1}; (2) the highest solubilized concentrations
376 of nutrient (TN = 2.0 g L^{-1}; PO_4^{3-} = 2.6 g L^{-1}) for resource recovery from the process water;
377 and (3) the best C utilization efficiency (70.2% in the hydrochar and 27.3% in the process
378 water). Although Mix_Citric exhibited the highest HHV and energy recovery efficiency (E_r =
379 0.50) and other superior energy-related properties due to the organic acid catalysis, the
380 pressurized environment, additional carbon source for repolymerization, high C loss of ~74%
381 into CO_2 form, and relatively low C utilization efficiency of citric acid catalyzed system
382 resulted in the overall higher carbon footprint with less environmental benefit. The critical
383 impacts of pressurized environment with different purging gases on the hydrochar properties
384 also warrant more attempts in the future studies. When recycling of process water is feasible,
385 co-HTC with ethanol-water system (Mix_Ethanol) or 0.5 M HNO_3 could be a feasible option
386 to effectively dissolve and oxidize biopolymers in the process water for enriched organic
387 carbon and lower aromaticity for bio-utilization. The downstream methane production,

possible inhibition on subsequent AD process due to residual catalyst and the intermediates, and potential eco-toxicity in environmental applications deserve future investigation.

To scale up the production of FWD and YW-derived hydrochar and ascertain the potential for fossil fuel replacement, it is necessary for future studies to develop deeper understanding on (1) the variation of FWD and YW properties with respect to the seasonal effect, and regional difference, and upstream AD operation conditions; (2) the overall energy balance, life cycle assessment (LCA), and techno-economic analysis (TEA) for the catalytic co-HTC process in comparison to the other available treatment technologies (*e.g.,* pyrolysis and composting); (3) the gas emissions and carbon capture/utilization during hydrochar combustion; and (4) the effects of recycling the catalyst and process water on the hydrochar properties.

4 Conclusions

Catalytic co-HTC process of FWD and YW can serve as a promising alternative to valorize FWD for bioenergy application and nutrient recovery towards circular economy and carbon neutrality. Compared with the non-catalytic hydrochar production, co-HTC with 0.5 M HCl maximized the added values for hydrochar as a solid fuel (HHV = 22.7 MJ kg^{-1}; 1.6-fold of FWD_DI) and nutrient recovery potential of process water, together with the attainment of the highest C utilization efficiency (97.5% overall). Further efforts on pilot-scale validation with material flow, energy balance, and overall environmental impacts are required to ensure practical feasibility for commercial applications.

Supplementary material

E-supplementary data for this study can be found in the e-version of this paper online.

Acknowledgement

The authors appreciate the financial support from the Hong Kong Environment and Conservation Fund (Project 101/2020) and Hong Kong International Airport Environmental Fund (Phase 2).

References

1. Ahmed, M., Andreottola, G., Elagroudy, S., Negm, M.S., Fiori, L., 2021. Coupling hydrothermal carbonization and anaerobic digestion for sewage digestate management: Influence of hydrothermal treatment time on dewaterability and bio-methane production. *Journal of Environmental Management*, **281**, 111910-111910.
2. Aragón-Briceño, C.I., Grasham, O., Ross, A.B., Dupont, V., Camargo-Valero, M.A., 2020. Hydrothermal carbonization of sewage digestate at wastewater treatment works: Influence of solid loading on characteristics of hydrochar, process water and plant energetics. *Renewable Energy*, **157**, 959-973.
3. Cao, Y., He, M., Dutta, S., Luo, G., Zhang, S., Tsang, D.C.W., 2021. Hydrothermal carbonization and liquefaction for sustainable production of hydrochar and aromatics. *Renewable & Sustainable Energy Reviews,* 152.
4. Coelho, J.J., Prieto, M.L., Dowling, S., Hennessy, A., Casey, I., Woodcock, T., Kennedy, N., 2018. Physical-chemical traits, phytotoxicity and pathogen detection in liquid anaerobic digestates. *Waste Management*, **78**, 8-15.
5. CRC., 2005. *CRC handbook of Chemistry and Physics*. CRC Press.
6. Deng, Y., Zhang, T., Clark, J.H., Aminabhavi, T., Kruse, A., Tsang, D.C.W., Sharma, B.K., Zhang, F., Ren, H., 2020. Mechanisms and modelling of phosphorus solid-liquid transformation during the hydrothermal processing of swine manure. *Green Chemistry*, **22**, 5628-5638.

7. Dincer, I., Rosen, M.A., Khalid, F., 2018. 3.16 Thermal Energy Production. in: *Comprehensive Energy Systems*, (Ed.) I. Dincer, Elsevier. Oxford, pp. 673-706.
8. Dutta, S., He, M., Xiong, X., Tsang, D.C.W., 2021. Sustainable management and recycling of food waste anaerobic digestate: A review. *Bioresource Technology*, **341**, 125915.
9. Faitli, J., Magyar, T., Erdélyi, A., Murányi, A., 2015. Characterization of thermal properties of municipal solid waste landfills. *Waste Management*, **36,** 213–221.
10. Faradilla, R.H.F., Lucia, L., Hakovirta, M., 2020. Remarkable physical and thermal properties of hydrothermal carbonized nanoscale cellulose observed from citric acid catalysis and acetone rinsing. *Nanomaterials*, **10**, 1049.
11. Lane, D.J., Truong, E., Larizza, F., Chiew, P., de Nys, R., van Eyk, P.J., 2018. Effect of hydrothermal carbonization on the combustion and gasification behavior of agricultural residues and macroalgae: Devolatilization characteristics and char reactivity. *Energy Fuels*, **32**, 4149-4159.
12. Lang, Q., Zhang, B., Liu, Z., Chen, Z., Xia, Y., Li, D., Ma, J., Gai, C., 2019. Co-hydrothermal carbonization of corn stalk and swine manure: Combustion behavior of hydrochar by thermogravimetric analysis. *Bioresource Technology*, **271**, 75-83.
13. Liu, H., Basar, I.A., Nzihou, A., Eskicioglu, C., 2021. Hydrochar derived from municipal sludge through hydrothermal processing: A critical review on its formation, characterization, and valorization. *Water Research*, **199**, 117186-117186.

14. Lucian, M., Volpe, M., Gao, L., Piro, G., Goldfarb, J.L., Fiori, L., 2018. Impact of hydrothermal carbonization conditions on the formation of hydrochars and secondary chars from the organic fraction of municipal solid waste. *Fuel*, **233**, 257-268.
15. Mäkelä, M., Yoshikawa, K., 2016. Ash behavior during hydrothermal treatment for solid fuel applications. Part 2: Effects of treatment conditions on industrial waste biomass. *Energy Conversion and Management*, **121**, 409-414.
16. Marin-Batista, J.D., Mohedano, A.F., Rodríguez, J.J., de la Rubia, M.A., 2020. Energy and phosphorous recovery through hydrothermal carbonization of digested sewage sludge. *Waste Management*, **105**, 566-574.
17. McCabe, A.J., Arnold, W.A., 2018. Multiple linear regression models to predict the formation efficiency of triplet excited states of dissolved organic matter in temperate wetlands. *Limnology and Oceanography*, **63**, 1992-2014.
18. Merzari, F., Goldfarb, J., Andreottola, G., Mimmo, T., Volpe, M., Fiori, L., 2020. Hydrothermal carbonization as a strategy for sewage sludge management: Influence of process withdrawal point on hydrochar properties. *Energies*, **13**, 2890.
19. Nicolae, S.A., Au, H., Modugno, P., Luo, H., Szego, A.E., Qiao, M., Li, L., Yin, W., Heeres, H.J., Berge, N., Titirici, M.-M., 2020. Recent advances in hydrothermal carbonisation: from tailored carbon materials and biochemicals to applications and bioenergy. *Green Chemistry*, **22**, 4747-4800.
20. Parmar, K.R., Ross, A.B., 2019. Integration of hydrothermal carbonisation with anaerobic digestion; Opportunities for valorisation of digestate. *Energies*, **12**, 1586.

21. Qian, L., Wang, S., Xu, D., Guo, Y., Tang, X., Wang, L., 2015. Treatment of sewage sludge in supercritical water and evaluation of the combined process of supercritical water gasification and oxidation. *Bioresource Technology*, **176**, 218-224.
22. Ro, K.S., Libra, J.A., Bae, S., Berge, N.D., Flora, J.R.V., Pecenka, R., 2019. Combustion behavior of animal-manure-based hydrochar and pyrochar. *ACS Sustainable Chemistry & Engineering*, **7**, 470-478.
23. Sharma, H.B., Dubey, B.K., 2020. Co-hydrothermal carbonization of food waste with yard waste for solid biofuel production: Hydrochar characterization and its pelletization. *Waste Management*, **118**, 521-533.
24. Sharma, H.B., Sarmah, A.K., Dubey, B., 2020. Hydrothermal carbonization of renewable waste biomass for solid biofuel production: A discussion on process mechanism, the influence of process parameters, environmental performance and fuel properties of hydrochar. *Renewable & Sustainable Energy Reviews*, **123**, 109761.
25. Smith, A.M., Singh, S., Ross, A.B., 2016. Fate of inorganic material during hydrothermal carbonisation of biomass: Influence of feedstock on combustion behaviour of hydrochar. *Fuel*, **169**, 135-145.
26. Sztancs, G., Kovacs, A., Toth, A.J., Mizsey, P., Billen, P., Fozer, D., 2021. Catalytic hydrothermal carbonization of microalgae biomass for low-carbon emission power generation: the environmental impacts of hydrochar co-firing. *Fuel*, **300**, 120927.
27. UNEP., 2021. Food waste index report 2021. United Nations Environment Programme.

28. Wilk, M., Śliz, M., Lubieniecki, B., 2021. Hydrothermal co-carbonization of sewage sludge and fuel additives: Combustion performance of hydrochar. *Renewable Energy*, **178**, 1046-1056.

29. Wyrzykowski, D., Hebanowska, E., Nowak-Wiczk, G., Makowski, M., Chmurzyński, L., 2011. Thermal behaviour of citric acid and isomeric aconitic acids. *Journal of Thermal Analysis and Calorimetry*, **104**, 731-735.

30. Xie, C., Liu, J., Zhang, X., Xie, W., Sun, J., Chang, K., Kuo, J., Xie, W., Liu, C., Sun, S., Buyukada, M., Evrendilek, F., 2018. Co-combustion thermal conversion characteristics of textile dyeing sludge and pomelo peel using TGA and artificial neural networks. *Applied Energy*, **212**, 786-795.

31. Xu, Z., He, M., Xu, X., Cao, X., Tsang, D.C.W., 2021a. Impacts of different activation processes on the carbon stability of biochar for oxidation resistance. *Bioresource Technology*, **338**, 125555-125555.

32. Xu, Z., Qi, R., Xiong, M., Zhang, D., Gu, H., Chen, W., 2021b. Conversion of cotton textile waste to clean solid fuel via surfactant-assisted hydrothermal carbonization: Mechanisms and combustion behaviors. *Bioresource Technology*, **321**, 124450-124450.

33. Yang, C., Wang, S., Yang, J., Xu, D., Li, Y., Li, J., Zhang, Y., 2020. Hydrothermal liquefaction and gasification of biomass and model compounds: A review. *Green Chemistry*, **22**, 821-8232.

514 34. Yang, J., Hong, C., Li, Z., Xing, Y., Zhao, X., 2021. Study on hydrothermal liquefaction
515 of antibiotic residues for bio-oil in ethanol-water system. *Waste Management*, **120**, 164-
516 174.
517 35. Yuan, X., He, T., Cao, H., Yuan, Q., 2017. Cattle manure pyrolysis process: Kinetic and
518 thermodynamic analysis with isoconversional methods. *Renewable Energy*, **107**, 489-496.
519 36. Zhang, C., Shao, M., Wu, H., Wang, N., Chen, Q., Xu, Q., 2021. Management and
520 valorization of digestate from food waste via hydrothermal. *Resources, Conservation and*
521 *Recycling*, **171**, 105639.
522 37. Zhang, J., Zhang, Y., 2014. Hydrothermal liquefaction of microalgae in an ethanol–water
523 co-solvent to produce biocrude oil. *Energy Fuels*, **28**, 5178-5183.
524 38. Zhang, T., He, X., Deng, Y., Tsang, D.C.W., Yuan, H., Shen, J., Zhang, S., 2020. Swine
525 manure valorization for phosphorus and nitrogen recovery by catalysis-thermal hydrolysis
526 and struvite crystallization. *Science of the Total Environment*, **729**, 138999.
527 39. Zheng, X., Ma, X., Hua, Y., Li, D., Xiang, J., Song, W., Dong, J., 2021. Nitric acid-
528 modified hydrochar enhance Cd^{2+} sorption capacity and reduce the Cd^{2+} accumulation in
529 rice. *Chemosphere*, **284**, 131261-13126.
530 40. Zhang, Z., Zhu, M., Zhang, D., 2018. A thermogravimetric study of the characteristics of
531 pyrolysis of cellulose isolated from selected biomass. *Applied Energy*, **220**, 87-93.

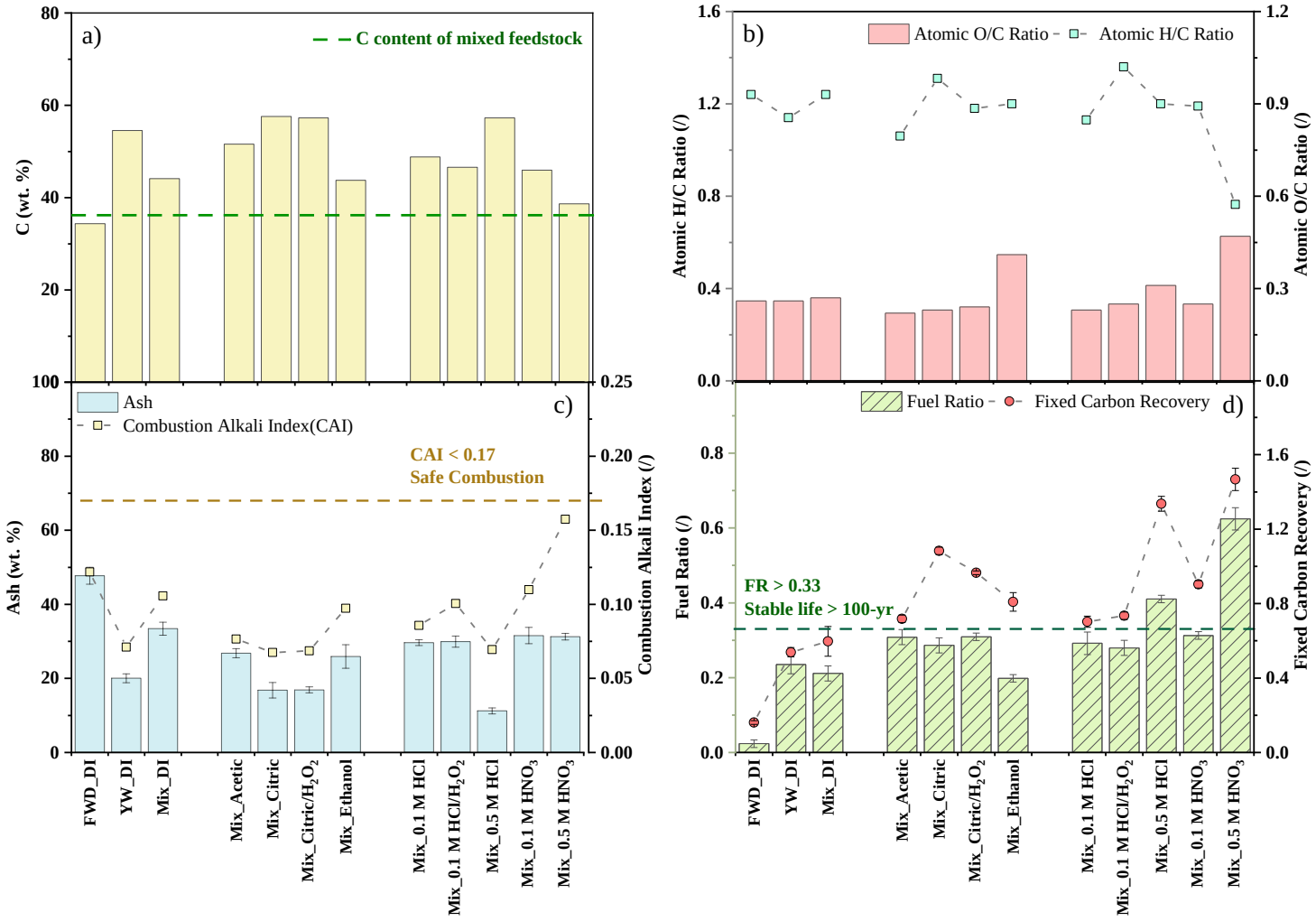

532 **Figure 1.** Carbon content of hydrochar (a); atomic H/C ratio and atomic O/C ratio of hydrochar

533 (b); ash content and combustion alkali index (CAI) of hydrochar (c); and fuel ratio and fixed

534 carbon recovery of hydrochar (d).

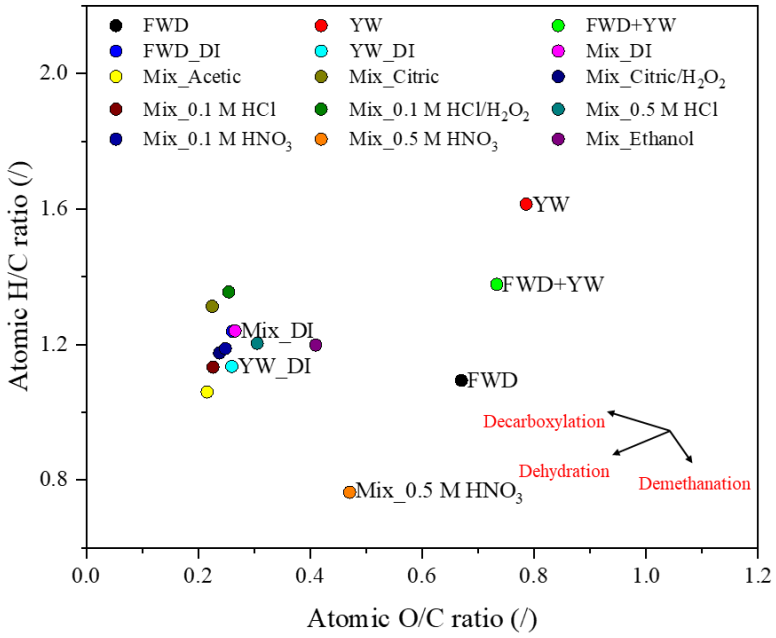

535

536 **Figure 2.** Van Krevelen diagram of hydrochar and FWD and YW feedstock.

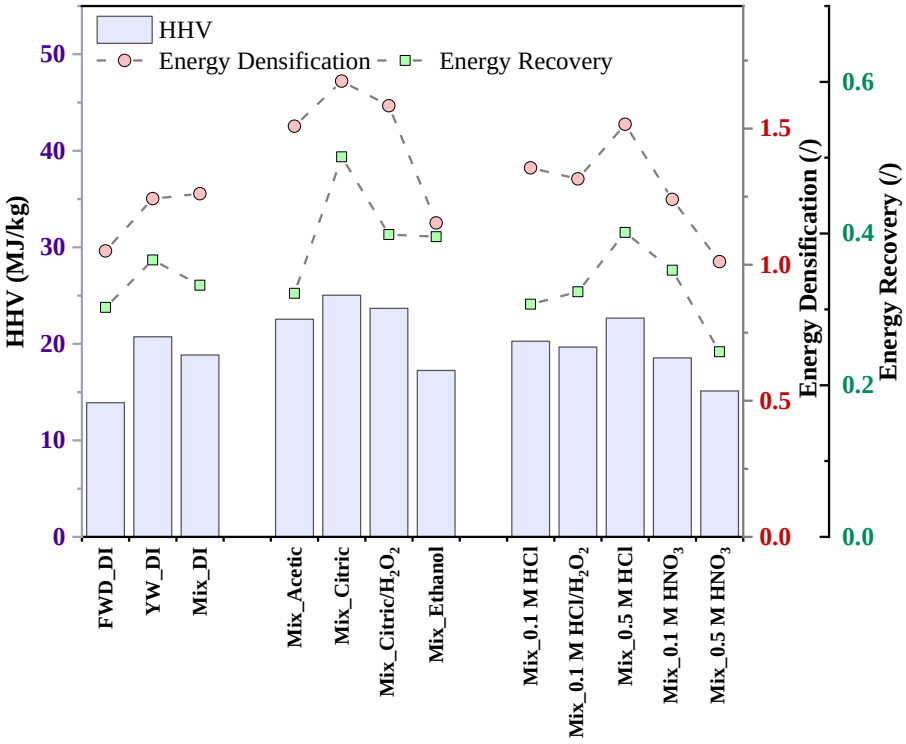

537

538 **Figure 3.** Higher heating value (HHV), energy densification, and energy recovery of

539 hydrochar.

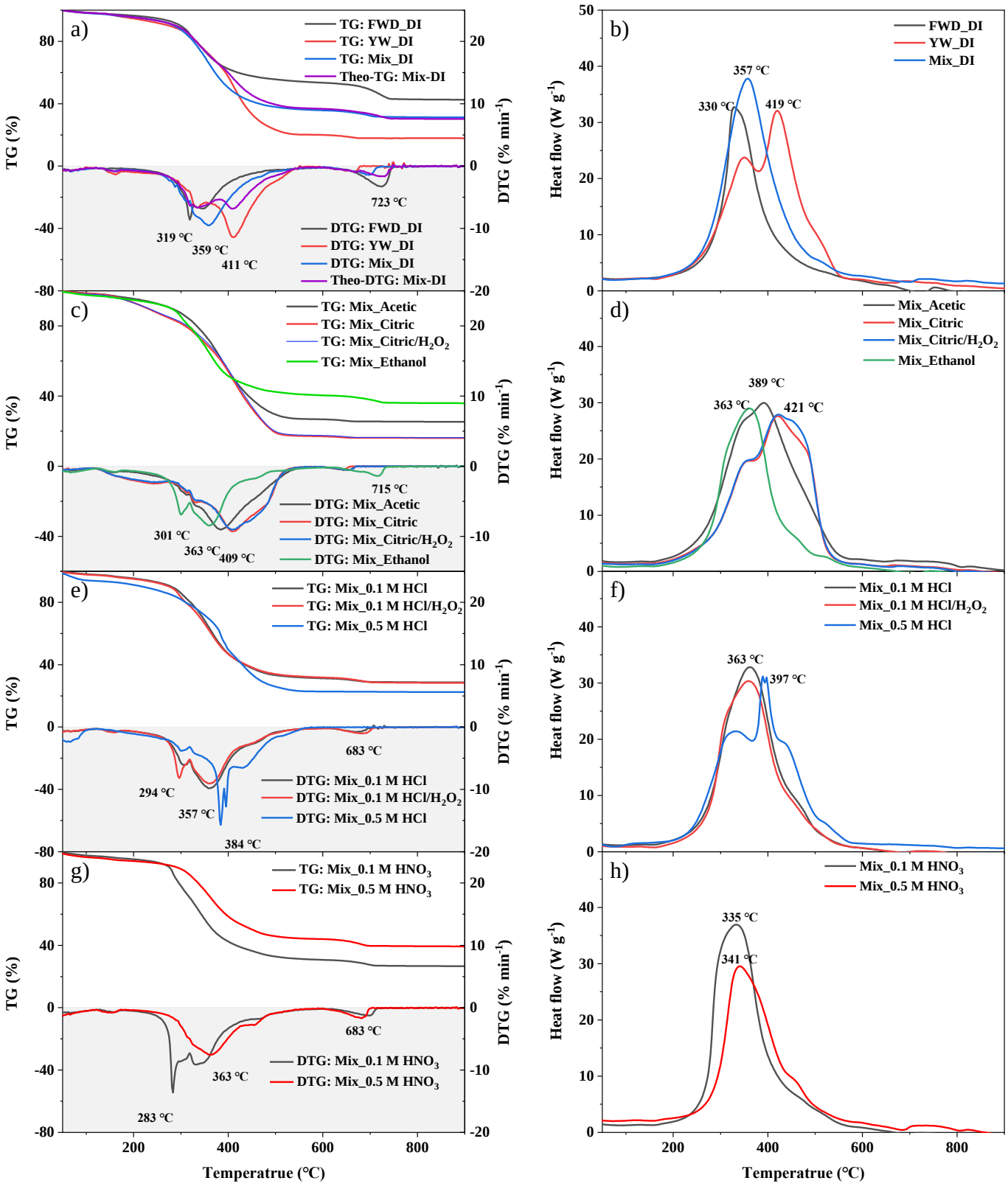

Figure 4. TG and DTG curves of hydrochar (a, c, e, and g); DSC curves of hydrochar (b, d, f, and h).

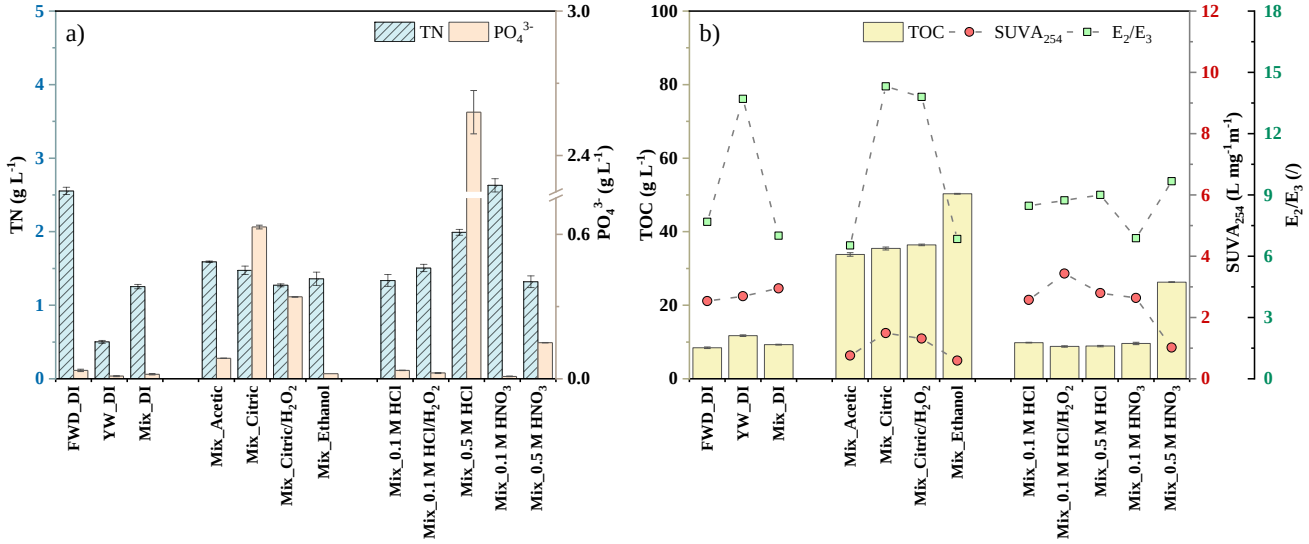

542

543 **Figure 5.** Total nitrogen (TN) and phosphate (PO_4^{3-}) of HTC process water (a); total organic

544 carbon (TOC), aromaticity ($SUVA_{254}$), and molecular weight (E_2/E_3) of HTC process water (b).

545

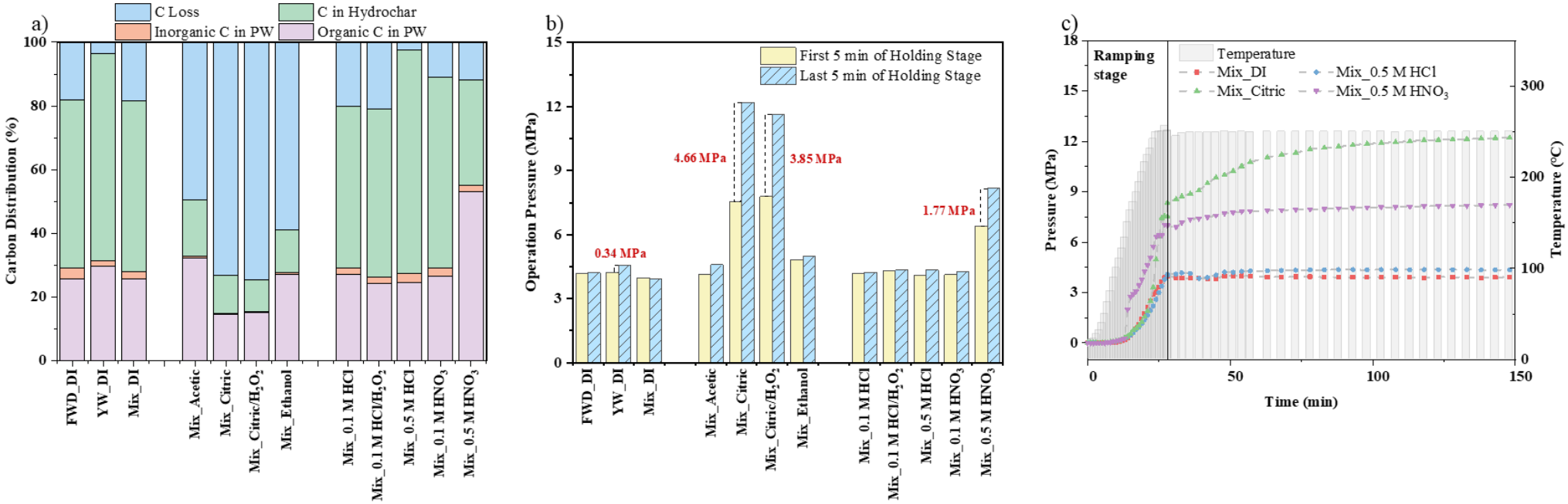

546

547 **Figure 6.** Carbon balance of HTC process (a); HTC operation pressures during the first 5 min and the last 5 min of holding stage (b); HTC

548 operation temperature and pressure during ramping and holding stage for hydrochar Mix_DI, Mix_0.5 M HCl, Mix_Citric, and Mix_0.5 M HNO_3

549 (c).

550 **Table 1.** Proximate and ultimate properties of feedstock and hydrochar

Feedstock	Moisture content (wt.% as received)	HHV (MJ kg^{-1})	Proximate analysis (wt.% dry basis)			Ultimate analysis (wt.% dry basis)				
			VM	FC	Ash	C	H	N	S	O
FWD	76.8	13.2	65.7	3.8	30.5	32.9	3.0	4.0	0.2	29.4
YW	35.0	16.7	74.1	13.3	12.6	39.4	5.3	1.0	0.5	41.3

Hydrochar	Proximate analysis (wt.% dry basis)			Ultimate analysis (wt.% dry basis)						
	VM	FC	Ash	C	H	N	S	O	H/C ratio [a]	O/C ratio [a]
FWD_DI	51.1	1.2	47.7	34.4	3.6	1.8	0.7	12.0	1.24	0.26
YW_DI	64.8	15.2	20.0	54.5	5.2	0.8	0.6	18.9	1.14	0.26
Mix_DI	55.0	11.6	33.4	44.1	4.6	1.7	0.6	15.7	1.24	0.27
Mix_Acetic	56.0	17.3	26.8	51.6	4.6	1.7	0.5	14.9	1.06	0.22
Mix_Citric	64.7	18.5	16.8	57.6	6.3	1.6	0.5	17.3	1.31	0.23
Mix_Citric/H_2O_2	63.5	19.6	16.9	57.3	5.6	1.6	0.5	18.2	1.18	0.24
Mix_Ethanol	61.9	12.3	25.9	43.7	4.4	1.7	0.4	23.9	1.20	0.41
Mix_0.1 M HCl	54.5	15.9	29.6	48.8	4.6	1.8	0.4	14.7	1.13	0.23
Mix_0.1 M HCl/H_2O_2	54.8	15.3	29.9	46.6	5.3	1.9	0.6	15.8	1.36	0.25
Mix_0.5 M HCl	63.0	25.8	11.2	57.5	5.8	1.6	0.5	23.4	1.20	0.31
Mix_0.1 M HNO_3	52.2	16.3	31.5	46.0	4.6	2.3	0.5	15.2	1.19	0.25
Mix_0.5 M HNO_3	42.3	26.4	31.2	38.6	2.5	3.3	0.1	24.2	0.76	0.47

551 [a] atomic ratio.

552

Table 2. Energy properties and combustion parameters of hydrochar

Sample	Solid yield (/)	HHV (MJ kg^{-1})	Energy densification (/)	Energy recovery (/)	DTG_m (% min^{-1})	DTG_{mean} (% min^{-1})	T_m (℃)	T_i (℃)	T_b (℃)	CCI (10^{-7} $\%^2$ min^{-2} $℃^{-3}$)	R_w (10^3)
FWD_DI	0.51	13.89	1.05	0.30	8.6	1.2	319	250	741	2.2	9.3
YW_DI	0.47	20.73	1.24	0.37	11.4	1.8	411	201	528	9.6	11.9
Mix_DI	0.44	18.85	1.26	0.33	9.6	1.6	359	240	707	3.8	9.6
Mix_Acetic	0.35	22.56	1.51	0.32	9.0	1.6	384	216	520	5.9	9.3
Mix_Citric	0.50	25.04	1.67	0.50	9.2	1.8	407	147	512	15.0	13.2
Mix_Citric/H_2O_2	0.42	23.68	1.58	0.40	9.0	2.0	407	147	515	16.2	12.9
Mix_Ethanol	0.56	17.25	1.15	0.40	8.4	1.4	361	235	724	2.9	8.5
Mix_0.1 M HCl	0.38	20.27	1.36	0.31	9.8	1.6	359	227	492	6.2	10.3
Mix_0.1 M HCl/H_2O_2	0.41	19.67	1.32	0.32	9.0	1.6	359	225	685	4.2	9.6
Mix_0.5 M HCl	0.44	22.66	1.52	0.40	15.6	1.8	384	193	530	14.2	18.1
Mix_0.1 M HNO_3	0.47	18.54	1.24	0.35	13.6	1.6	283	238	705	5.4	17.3
Mix_0.5 M HNO_3	0.40	15.11	1.01	0.24	7.6	1.4	363	264	693	2.2	6.8

553

554